Single-cell nanocapsules of gut microbiota to facilitate fecal microbiota transplantation

Weiliang Hou[1,2,3,4]✉, Yuan Cao[5,6], Jifeng Wang[6], Fang Yin[1], Jiahui Wang[1], Ning Guo[1], Ziyi Wang[4], Xiaoqiong Lv[7], Chunlian Ma[7], Qiyi Chen[7], Rong Yang[8], Hong Wei[9], Juanjuan Li[10]✉, Ruibing Wang[4]✉, Huanlong Qin[1]✉

[1]Research Institute of Intestinal Diseases, Shanghai Tenth People's Hospital Affiliated to Tongji University, 200072 Shanghai, China.

[2]Department of Gastroenterology, Shanghai Institute of Pancreatic Diseases, Changhai Hospital; National Key Laboratory of Immunity and Inflammation, Naval Medical University, 200433 Shanghai, China.

[3]Shanghai Cancer Institute, Renji Hospital School of Medicine, Shanghai Jiao Tong University, 200030 Shanghai, China.

[4]State Key Laboratory of Quality Research in Chinese Medicine, Institute of Chinese Medical Sciences, University of Macau, SAR 999078 Taipa Macau, China

[5]Institute of Clinical Science, Zhongshan Hospital, Fudan University, 200032 Shanghai, China

[6]Department of Pathology, Shanghai Tenth People's Hospital Affiliated to Tongji University, 200072 Shanghai, China.

[7]Intestinal Microenvironment Treatment Center, Shanghai Tenth People's Hospital Affiliated to Tongji University, 200072 Shanghai, China.

[8]Department of Pediatrics, Shanghai Tenth People's Hospital Affiliated to Tongji University, 200072 Shanghai, China.

[9]Central Laboratory, Clinical Medicine Scientific and Technical Innovation Park, Shanghai Tenth People's Hospital Affiliated to Tongji University, 200435 Shanghai, China.

[10]School of Life Sciences, Hainan University, 570228 Haikou, China.

First Authors: Weiliang Hou, Yuan Cao, Jifeng Wang and Fang Yin contributed equally to this work.

✉ Corresponding authors: Weiliang Hou (houweiliang@tongji.edu.cn) or Juanjuan Li (lijuanjuan@hainanu.edu.cn) or Ruibing Wang (rwang@um.edu.mo), or Huanlong Qin (huanlong_qin@live.cn).

Abstract

Rationale: Fecal microbiota transplantation (FMT) presents great advantage for treating intractable diseases by microbiota-gut-organ axis. However, the invasive administration of gut microbiota by nasal feeding tube limits the widespread application of FMT. Herein, we attempt to develop a novel strategy to deliver gut microbiota by nanocapsules.

Methods: Single cell nanocapsules were hence implemented by the layer-by-layer assembly of silk fibroin and phosphatidylcholine to generate the protection nanoshell on the cell surface of complicated microbiota within 1 hour. The physical properties of microbiota nanocapsules were analyzed. The protective effects of nanocapsules against gastrointestinal tract were demonstrated in vitro and in vivo. The efficacy of FMT assisted by single-cell nanocapsules (NanoFMT) was evaluated by inflammatory response, gut microbiota balance and histopathology analysis in animal model.

Results: Nanocapsules achieved well coating ratio for single kind of microbe and complex microbiota, resulting in remarkable reinforcement on survival rate of microbes in gastrointestinal tract. NanoFMT better improved the diversity and abundance of gut microbiota than common FMT in germ free mice. Moreover, NanoFMT superiorly alleviated intestinal inflammation and positively reversed microbiota balance in mouse model of colitis compared with common FMT, assisted by the inherent anti-inflammation of silk fibroin and phosphatidylcholine.

Conclusions: Considering rapid preparation, convenient delivery and perfect

therapeutic effect, we anticipate NanoFMT could be a promising clinical candidate for the next-generation FMT treatment.

Keywords: Single-cell nanocapsules, Microbial therapy, NanoFMT, Gut microbiota, Colitis

Graphical Abstract

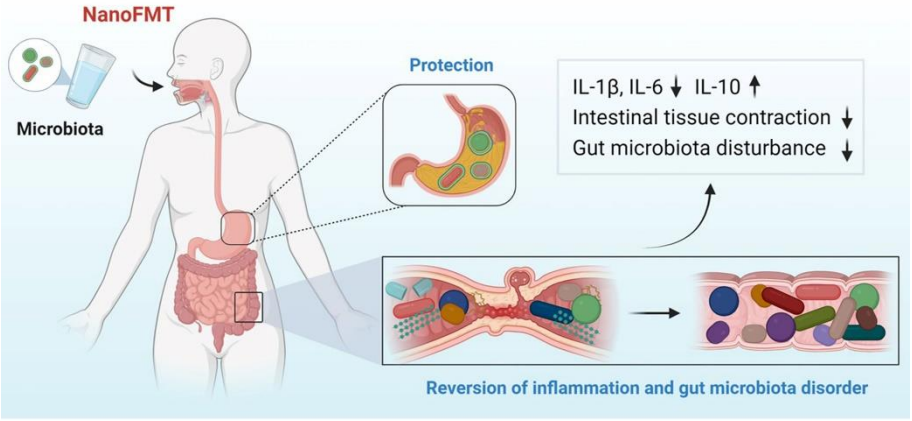

Introduction

Gut microbiota plays a pivotal role in regulating human health from multiple aspects [1-3]. Accordingly, fecal microbiota transplantation (FMT) has become a therapeutic strategy by transferring gut microbiota from a rigorously screened healthy donor to a diseased recipient for treating diseases such as diabetes mellitus, hypertension, inflammatory bowel disease (IBD), obesity, etc [4-7]. Initially, microbiota slurries are prepared by homogenization and filtration of fecal material under sterile conditions and then administered by invasive nasogastric feeding tube or colonoscopy [8-10], which is unfriendly for children and the elderly. Fecal microbiota capsules were hence developed by freeze-drying of microbiota slurries for around 24 h under -80 ^{o}C, suitable for oral administration [11-13]. However, complicated preparation procedure of microbiota capsules could decrease microbial activity and increase manufacturing cost of microbiota product in a certain extent [14]. Therefore, it is imperative to develop next generation FMT technology occupied with concurrently oral convenience and high microbial activity.

Surface modification has been utilized in microbial therapy to introduce exogenous functions [15-17]. By the entire coating on bacterial surface, nanocoated bacteria usually show improved bioavailability, controlled release profile, and enhanced pharmaceutical effects when compared to capsules packaging [18, 19]. Recently, various coatings were attempted to increase bacterial survival and colonization in vivo [20-22]. For instance, coating living bacteria with polydopamine nanoparticular immunosuppressant could strengthen bacterial viability in

gastrointestinal tract, suppress hyperactive immune response and modulate gut microbiome [23]. Current studies mostly coated mono-microbe such as *Escherichia coli*, *Saccharomyces cerevisiae* and *Listeria monocytogenes* [24-26]. It is considered extremely challenging to coat microbiota containing thousands of kinds with diverse surface structures [27].

When used in FMT treatment, rapid preparation, high activity, well protection and low toxicity are needed to coat gut microbiota. However, few studies could meet these requirements. Dopamine could polymerize on the surface of bacteria to achieve gastrointestinal protection, but perhaps decreasing bacterial activity due to the high pH environment during polymerization [20]. Silk fibroin could generate nanoshell by conformation transition from a random coil to β-sheet conformation under moderate conditions, while well protection need up to four layers coating of silk fibroin [22]. Herein, we firstly report a novel single-cell nanocapsules to coat gut microbiota by the layer-by-layer self-assembly. Silk fibroin firstly self-assembled on the surface of gut microbiota to generate nanoshell, sequentially phosphatidylcholine was used to reinforce the nanoshell by electrostatic adsorption. The nanocoating could be completed within 1 hour and achieve a high coating ratio of gut microbiota, yet no impacting the activity of microbiota. The remarkable protection of nanocapsules was demonstrated in vitro and in vivo, resulting in the improved abundance and diversity of gut microbiota in germ-free mice after FMT. The excellent therapeutic efficacy of FMT assisted by single-cell nanocapsules (NanoFMT) was observed in mouse model of colitis compared

with that of regular FMT. Moreover, silk fibroin and phosphatidylcholine are both approved by Food and Drug Administration (FDA). Considering clinical safety, convenient preparation and perfect therapeutic effect, we anticipate that NanoFMT could innovate the current avenue of FMT to achieve more convenient and widespread clinical application.

Materials and Methods

Materials and strains

Escherichia coli Nissle 1917 (EcN) was purchased from the China General Microbiological Culture Collection center (CGMCC) and grown in Luria Bertani (LB) medium at 37 °C with suitable antibiotics. *Pediococcus acidilactici* DQ2 (PA) was stored at CGMCC with the registration number of 7471 and grown in Man-Rogosa-Sharp medium. Cholic acid, pepsin and phosphatidylcholine were purchased from Adamas. Dextran sulfate sodium (reagent grade; MW 36-50 kDa) was obtained from Sangon.

Preparation of silk fibroin

Silk fibroin solution was prepared as previously described [28]. Briefly, cocoons were boiled in 0.02 M sodium bicarbonate for 20 min and then rinsed thoroughly using Nanopure water. The extracted silk fibroin was dissolved in 9.3 M LiBr solution at 60 °C for 4 h, followed by dialyzing against Nanopure water using a Slide-a-Lyzer dialysis cassette (molecular weight cutoff 3500 Da, Pierce) at room temperature. The dialysate was centrifuged three times, each for 20 min, followed by filtering using a 0.4

μm glass-fiber syringe filter. The silk fibroin concentration was diluted to 0.1% (w/v) by Nanopure water.

Preparation of single-cell nanocoated microbes

Cultured EcN were washed three times using 0.01 M sodium phosphate buffer (pH 6.0) and centrifuged at 10000 rpm, followed by adding 0.1% (w/v) silk fibroin under shaking at 35 rpm for 10 min. Afterward, cells were centrifuged, washed by Nanopure water, resuspended in 0.1 M potassium phosphate buffer (pH 5.5) and then incubated by vigorous shaking on Vertex (1000 rpm) for 10 min. Silk fibroin coated EcN was centrifugated, washed and resuspended in 5 mg/mL phosphatidylcholine and incubated by vigorous shaking for 10 min. The final coated cells were named as NanoEcN. PA cells and SC cells were also coated by the above steps. Gut microbiota was obtained by collecting fresh mouse fecal in sterile normal saline and filtering using 70 μm pore nylon filter to remove large particulate and fibrous matter. Gut microbiota was successively coated by silk fibroin and phosphatidylcholine, and tentatively stored in 4 °C.

Characterization of single-cell nanocoated microbes

Silk fibroin labeled by fluorescein isothiocyanate (FITC) and phosphatidylcholine labeled by rhodamine B on the surface of nanocoated microbe cells was observed by laser scanning confocal microscopy (Leica TCS SP8, German). The percentage of nanocoated microbe cells was examined by flow cytometry (Beckman CytoFlex, USA). The morphology of microbes was visualized by transmission electron microscopy

(TEM) (HITACH, Japan) and atom force microscopy (AFM) (Dimension FastScan Bio, Bruker, USA).

Resistance assessment in vitro

An equal amount of nude microbes or nanocoated microbes was resuspended into 1 mL medium containing simulated gastric fluid (SGF) with 10 g/L of pepsin in 0.85% NaCl solution (HCl) for two hours at 37 ℃, then diluted and spread onto agar plate. Microbes were inoculated in simulated intestinal fluid (SIF) with trypsin in KH_2PO_4 solution, cholic acid (CA) solution or the corresponding culture media at 37 °C for the predetermined time points. The nude microbes and nanocoated microbes were stored in 4 ℃ for 7 days to evaluate the stability of nanocapsules by TEM images.

Adhesion observation in vitro

The mouse colon was cut into small sections and incubated with 3% dextran sulphate sodium (DSS) for 48 h at 37 °C to simulate mucus injury. After 4′,6-diamidino-2-phenylindole dihydrochloride (DAPI) staining, EcN or NanoEcN (10^7 colony forming units (CFU)/mL) was added under mild shake for 20 min, then PBS washing for imaging or colony counting.

In vitro assessment of anti-inflammation properties

RAW 264.7 macrophage cells were cultured in 24 well (DMEM medium) at 37 °C for 24 h and washed by PBS. Subsequently, silk fibroin (0-20 μg/mL) or phosphatidylcholine (25 μg/mL) were cultured with RAW 264.7 cells in the absence or presence of lipopolysaccharide (LPS) (1 μg/mL) for 24 h. Supernatant liquid was used

for measuring NO content and cytokine level while cultured RAW 264.7 cells were labeled by ROS probe (10 μM DCFH-DA) for flow analysis or confocal imaging, or stained with FITC-conjugated anti-CD86 antibody to analysis M1 macrophage polarization by flow analysis.

Cell safety evaluation

Caco-2 cells were seeded in 96 well (DMEM medium) at 37 °C for 24 h, washed by PBS, subsequently adding new DMEM medium containing phosphatidylcholine or silk fibroin solution for another 24 h. Thiazolyl blue (MTT) (0.5 mg/mL) was supplemented in medium under dark condition for 1 h. Then the medium was removed, and the wells were filled with Dimethyl sulfoxide for absorbance measurement at 570 nm. Cell counting Kit-8 (CCK8) was supplemented in medium under dark condition for 1 h to measure absorbance at 450 nm.

Animals

SPF Balb/c mice (male, 6 weeks) were purchased from Jiesijie Laboratory Animal Technology. Germ-free (GF) KM mice (male, 6 weeks) were obtained from the Department of Laboratory Animal Science of Tenth People Hospital of Tongji University and bred in a gnotobiotic environment. All the animal procedures were complied with the guidelines of the Shanghai Medical Experimental Animal Care. Animal protocols were approved by the Institutional Animal Care and Use Committee of Shanghai Tenth People Hospital (SHDSYY-2021-6483).

Oral bioavailability in SPF mice

Six-week-old male Balb/c mice were randomly divided into 2 groups (n = 6) and fed with 2×10^7 CFU/mouse EcN or NanoEcN by oral gavage. At 4 h or 120 h post-administration, mice were sacrificed and the intestinal tracts were harvested, imaged by in vivo imaging system (IVIS Lumina II, Caliper) and colony counted in plate with suitable antibiotics.

Gut microbiota distribution in GF mice

Six-week-old male GF KM mice were randomly divided into 2 groups (n = 4) and treated with FMT (2×10^6 CFU/mouse) or NanoFMT (2×10^6 CFU/mouse). At 24 h post-administration, mice were sacrificed and feces samples were collected for 16S rRNA gene sequencing. The total DNA was extracted form colonic content and sequenced by building sequencing library on Illumina HiSeq 2500. The original image data files obtained by high-throughput sequencing were converted into Sequenced Reads by Base Calling analysis. The results were stored in FASTQ format file. Data analysis was performed on BMKCloud for species diversity, abundance and community structure.

Salmonella typhimurium -induced colitis model

The *Salmonella typhimurium* (STm)-induced colitis was established as described previously [29]. Balb/c mice (male, 6-8 weeks) were treated with 100 μl of streptomycin solution (200 mg/mL) prior to infection by orally inoculating with 1×10^9 CFU of *Salmonella*. Mice were randomly divided into 3 groups (n = 5) and treated with PBS, FMT (2×10^7 CFU/mouse/day) and NanoFMT (2×10^7 CFU/mouse/day) at day

2 and 4 post-infection, respectively. Mice were weighted every day and sacrificed at day 6 post-infection. The inflamed colon of the mice was sampled for blinded histopathology analysis and mouse blood was collected to prepare serum samples by centrifugation for cytokines level detection by ELISA kits.

DSS-induced colitis model

Balb/c mice (male, 6-8 weeks) were fed with 3% DSS salt in sterile drinking water for 7 days. Mice were randomly divided into 3 groups (n = 5) and then administered with PBS, FMT (2×10^7 CFU/mouse/day) or NanoFMT (2×10^7 CFU/mouse/day) by gavage for 5 days. On day 6, mice were orally administrated with 600 mg/kg mouse FITC-dextran. After 4 h, mice were sacrificed. The serum samples were used for measuring cytokines by commercially available ELISA kits (MultiSciences Biotech, China), and intestinal permeability by photometric analysis at excitation wavelength of 4855 nm and an emission wavelength of 528 nm. The colon of the mice was sampled for blinded histopathology analysis.

In-vivo biosafety assessment

Balb/c mice (male, 6-8 weeks) were randomly divided into 2 groups (n = 6) and orally administrated with PBS or NanoFMT (2×10^7 CFU/mouse/day) daily. After 14 days, mice were sacrificed, and blood and organ were used for hematological analysis and histopathology analysis, respectively.

Histopathology analysis

Tissue samples were fixed in 4% formalin, embedded in paraffin according to

standard procedures, and then sectioned at 4 μm for hematoxylin and eosin (H&E) staining and myeloperoxidase (MPO) staining. All of the images of the tissues were captured by 3D HISTECH Pannoramic 250 (3DHISTECH, Hungary).

Data analysis

We used 3 independent samples in the in vitro experiments and at least 4 independent samples in animal experiments. We analyzed data by IBM SPSS software, and compared samples between groups with ANOVA and made multiple comparisons by least-significant difference method. The value of $p < 0.05$ was considered to be statistically significant.

Results

Fabrication of single-cell nanocapsules

Silk fibroin, a natural polymer, has been used as biomaterial approved by FDA due to its biocompatibility, biodegradability, non-immunogenicity, and innate anti-inflammatory effect. Interestingly, silk fibroin could self-assemble into protective nanoshells on the surface of different nanoparticles by its transition from a random coil to β-sheet conformation, which has been studied for potential drug delivery [30]. We found that four layers of silk fibroin could achieve well coating of microbes [22], yet which was too tedious for coating complex microbiota, perhaps causing the substantial loss of microbial activity. Phosphatidylcholine is largely responsible for establishing a protective hydrophobic surface and therefore plays a key role in mucosal defence [31]. Due to its zwitterionic nature, phosphatidylcholine may form nanoshell by electrostatic

adsorption with silk fibroin. Accordingly, we designed a layer-by-layer strategy to coat gut microbiota by silk fibroin and phosphatidylcholine for making single-cell nanocapsules to improve gastrointestinal survival of fecal microbiota (Figure 1).

Gut microbiota mainly includes gram-negative bacteria, gram-positive bacteria and fungi [32], whose cell wall present different structure features of cell wall, perhaps impacting the nanocoating ratio of silk fibroin and phosphatidylcholine. Therefore, we firstly chose three representative probiotics for evaluating the feasibility of single-cell nanocapsules for coating microbiota, including gram-negative bacteria EcN, gram-positive bacteria PA and fungi *Saccharomyces cerevisiae* (SC). Silk fibroin was prepared by extraction from cocoons in a boiling solution of 0.02 M sodium bicarbonate. The resulting silk fibroin was purified by stirring in 9.3 M LiBr at 60 °C for 4 h and subsequently dialyzed against substantial Nanopure water at room temperature. Microbes were simply shaken with 0.1 % silk fibroin solution for 10 min to generate β-sheet conformation from a random coil and subsequently vigorously shaken in 0.1 M K^+ phosphate buffer (pH 5.5) for an additional 10 min to stabilize the formed coating by a salting-out process [33]. Silk fibroin coated microbes were vigorously shaken in 5 mg/mL phosphatidylcholine for 10 min to form the completed nanocoating via electrostatic adsorption. Silk fibroin coated microbes and the finally coated microbes were respectively renamed by adding the prefix S and Nano (Figure S1). Dynamic light scattering showed that particle size of microbes presented an increase tendence with the coating process (Figures 2A-C), while zeta potential of microbes only slightly

decreased due to electronegative property of silk fibroin and zwitterionic nature of phosphatidylcholine (Figures 2D-F). The results indicated that a desired nanocoating could be acquired using the layer-by-layer strategy by silk fibroin and phosphatidylcholine sequentially. Subsequently, we detailedly observed the morphological difference of microbes and their nanoderivatives using TEM and AFM. A remarkable increase in the surface thickness and roughness of EcN after coating by silk fibroin and phosphatidylcholine was displayed compared with the nude one (Figure 2G and Figure S2). The similar morphological change was also found in PA, SC and their nanoderivatives, demonstrating that single-cell nanocapsules could coat the different kinds of microbes.

After successfully coating gram-negative bacteria, gram-positive bacteria and fungi, we further attempted to fabricate single-cell nanocapsules of complex gut microbiota by the layer-by-layer strategy. Gut microbiota was prepared by homogenate and filtration of mouse feces using 70 μm pore nylon filter to remove the large impurities. The fecal filtrate containing various microbiota was sequentially coated by silk fibroin and phosphatidylcholine. As the impurities interferences from the fecal filtrate (such as neutral fiber, and negatively charged proteins) could impact charge measurement and difficult identification of the microscopic images from the nanocoated microbiota and the nude one, we attempted to assess the coating efficacy of gut microbiota by fluorescently labeling the nanoshell. Silk fibroin and phosphatidylcholine were respectively labeled by FITC and rhodamine B. Confocal

images showed that the fluorescence signal of FITC and rhodamine B sequentially merged with the coating process of single kind of microbe (Figure 2H and Figures S3A-C). The similar fluorescence images exhibited in the fabrication process of single-cell nanocapsules of gut microbiota (Figure 2H and Figure S3D), hence elucidating that the layer-by-layer strategy could coat complex gut microbiota. Quantitative analysis by flow cytometry suggested the coating ratio of microbiota could reach up to 74.4% using the layer-by-layer strategy, which was consistent with that of single kind of microbe (Figure 2I). Importantly, high retrieval rate of microbes still kept after twice decorating (Figure S4). Collectively, these results demonstrated that the layer-by-layer strategy using silk fibroin and phosphatidylcholine could achieve excellent coating to prepare single-cell nanocapsules of complex gut microbiota.

The impact of nanocapsules on gastrointestinal tolerance, intestinal adhesion and anti-inflammation in vitro

One may speculate that nanocoating could potentially impact on microbe bioactivity. We firstly measured strain growth after the layer-by-layer coating. Interestingly, the growth of NanoEcN, NanoPA, NanoSC and NanoMicrobiota was similar with the nude ones, indicating that the layer-by-layer coating by silk fibroin and phosphatidylcholine did not disturb microbes growth and strains could proliferate by breaking the nanoshell (Figures 3A-D and Figure S5).

Most of microbes would be dead under acid attack and pepsin enzymolysis in stomach after oral administration without nanoencapsulation. In order to investigate the

protective effects of the nanocapsules on microbiota, we firstly examined the tolerance of nanocoated microbes in SGF with 10 g/L of pepsin in 0.85% NaCl solution (HCl, pH 2.5). The same quantity of nanocoated microbes and the nude ones were respectively incubated in the simulated gastric acid at pH 2.5 for 2 h. The survival of nanocoated microbes significantly improved an order of magnitude compared with the nude versions of EcN, PA and SC, which was similar in SGF with different pH (Figures 3E-G and Figures S6-7). Especially, the bacterial count of NanoMicrobiota increased 20.5 folds than the nude microbiota (Figure 3H). TEM images demonstrated that the nanocoated microbes kept morphological integrity while the nude one present the broken state (Figure 3I). The microbe growth was also evaluated in SIF. The nanocoated microbes presented a faster growth rate than the nude one in the early stage, which was in consistent with the results in SIF with different trypsin content (Figures S8-9). CA from intestinal tract could deactivate microbes. We hence evaluated the resistance of microbes against CA (0.3 mg/mL) and found that nanocapsules well armed microbes with the highest activity up to 1.7 folds than the nude one (Figure S10). The advantage of nanocapsule coated microbes was further presented with the increase of CA concentration (Figure S11). Moreover, nanocapsules showed well stability in long-term storage (Figure S12). These results suggested that nanocapsules constructed by silk fibroin and phosphatidylcholine could potentially protect microbes from the assaults of gastrointestinal tract.

Intestinal adhesion is one of the key factors influencing microbial intestinal

colonization. We constructed a DSS damaged colon to assess microbial intestinal adhesion on inflamed intestine in vitro. Nanocapsules significantly improved intestinal adhesion of EcN with the 1.5-fold increased count compared with the nude one after 30 min co-incubation with inflamed intestine (Figures 3J-K), perhaps due to the elevated particle size and surface area given by nanocoating.

Anti-inflammation is the critical pathway to treat intestinal inflammation. We investigated the anti-inflammation properties of nanocapsules components, silk fibroin and phosphatidylcholine. RAW 264.7 macrophage cells were cultured in DMEM medium with 1 μg/mL LPS and silk fibroin or phosphatidylcholine for 24 h, then ROS level, NO content and percentages of CD86+ macrophages were analyzed in RAW 264.7 cells. LPS could induce the generation of ROS and NO and lead to macrophage polarization. We found that silk fibroin and phosphatidylcholine both significantly weakened ROS generation, while silk fibroin achieved better ROS elimination with 2.6-fold reduction than LPS induction (Figures 3L-M and Figure S13A). Interestingly, silk fibroin and phosphatidylcholine also decreased NO content in RAW 264.7 cells after exposure to LPS (Figure 3N and Figure S13B). LPS could induce M1 phenotype macrophage polarization in RAW 264.7 cells, which was prohibited by silk fibroin and phosphatidylcholine, as reflected by the decreased expression of CD86 (Figure 3O and Figure S13C) and the reversed cytokine level (Figure S14). The cell toxicity of nanocapsules was investigated in intestinal cells and significant decrease of cell viability was not found by MTT and CCK8 methods in Caco-2 cells after exposure to

silk fibroin and phosphatidylcholine (Figure S15). These results indicated that nanocapsules provided extra anti-inflammation effect and did not damage intestinal cell.

Nanocapsules mediated the efficiency of intestinal colonization and FMT

We further investigated the protection of microbes by nanocapsules in real gastrointestinal tracts. EcN with red fluorescence was used as the model microbe for monitoring bacterial intestinal engraftment (Figure 4A). Mice were orally administered with EcN and sacrificed for imaging at 4 h post administration. The fluorescence intensity of EcN was imaged by IVIS. Compared with nude EcN, nanocoated EcN more accumulated in the abdominal region (Figures 4B-C). Anatomic analysis showed that EcN distributed well in the intestine and cecum of mice treated with the nanocoated microbes more than those of the nude trains (Figures 4D-E). Interestingly, the increased counting of EcN by nanocapsules respectively reached to 8.9 folds in small intestine, 3.1 folds in cecum and 2.4 folds in colon comparing with that of the nude EcN (Figures 4F-I), indicating that nanocapsules significantly improved the intestinal engraftment of EcN. Further, we found that the colonization of nanocapsule coated EcN still presented a great advantage relative to that of EcN in gastrointestinal tract after oral administration on day 5 (Figure S16).

To further investigate the impact of nanocoating on gut microbiota's engraftment, we prepared NanoMicrobiota using microbiota isolated from healthy mice. Nude microbiota and NanoMicrobiota were orally administered into germ-free mice for FMT and NanoFMT, respectively. Mouse feces were collected after 24 h post gavage and

measured by 16S ribosomal RNA gene sequencing (Figure 4J). Venn diagram showed that 674 operational taxonomic units (OTUs) were shared by the NanoFMT and FMT groups, while the specific OTUs from NanoFMT group increased by 383 than that from FMT group, indicating that the nanocoating significantly improved the survival rate of gut microbiota in mice (Figure 4K). NanoFMT group presented higher alpha diversity than FMT group and significantly separated beta diversity with FMT group (Figures 4L-M). Relative abundance of gut microbiota presented uniformity in the phylum and genus levels between samples in NanoFMT group, indicating a better repeatability of FMT by nanocapsules (Figures 4N-O and Figure S17). *Bacteroides*, keystone species in gut, were 14.5 thousand folds higher in NanoFMT group than those of FMT group (Figure 4P). *Lactobacillus* associated with the recovering of IBD showed a much higher relative abundance in NanoFMT group [34], manifesting that better inflammatory reversion could be achieved by NanoFMT (Figure 4Q). *Parabacteroides* have the physiological characteristics of carbohydrate metabolism and secret short chain fatty acids [35], which only survived in NanoFMT group (Figure 4R). Collectively, these results indicated that nanocapsules could significantly ameliorate the resistance of microbes from the microenvironment of gastrointestinal tract, and hence increasing the overall microbial survive rate and microbiota diversity.

NanoFMT for regulating gut microbiota and reversing intestinal inflammation

We subsequently examined the therapeutic effect of NanoFMT in colitis mouse model induced by STm. Mice were administered with streptomycin one day before

STm infection, and then orally administered with gut microbiota nanocapsules for NanoFMT on day 2 and 4 post-infection. Common FMT and PBS treatment were employed as the control and blank, respectively. Subsequently, mice were sacrificed on day 5 post-infection for analyzing intestinal tissues and serum (Figure 5A). Some mice were dead from PBS group on day 3 and 4 post-infection, while the death rate of FMT group was relatively lower, but still reached to the same mortality rate with that of PBS group on day 5 post-infection (Figure 5B). Conversely, no mice were dead in NanoFMT group, indicating the best therapeutic effect of NanoFMT. We hence investigated specific mechanism of NanoFMT on the treatment of STm-induced colitis. STm infection could cause severe inflammation in intestinal tract, hence shortening the intestinal length [36]. FMT alleviated inflammation and recover intestinal length to a certain extent, while NanoFMT group exhibited the longest colon length (Figure 5C and Figure S18). The cytokine levels were investigated by ELISA kits. Remarkably, NanoFMT reversed the cytokine levels of interleukin-1β (IL-1β) and interleukin-6 (IL-6) in the serum, in a more pronounced manner than FMT, indicating the superior improvement of the systemic inflammation by NanoFMT (Figures 5D-E). Previous studies have demonstrated that silk fibroin and phosphatidylcholine both presented the inherent anti-inflammatory effects in animal model and clinical application [37]. Nanocapsules formed by silk fibroin and phosphatidylcholine could moderate intestinal inflammation, except providing gastrointestinal protection. Histopathological analysis of colon tissue was performed using H&E staining and MPO staining (Figure 5F). As

expected, NanoFMT obviously mitigated inflammation and hemorrhage of the colon, while significantly fewer MPO positive cells were observed in the colon lesions in NanoFMT group than those of FMT group.

As NanoFMT remarkably ameliorated gut microbiota of germ-free mice (Figure 4), we further analyzed the impact of NanoFMT on gut microbiota of STm-induced colitis. Venn diagrams showed the number of shared OTUs was 212 in the three groups (Figure 6A). The unique OTUs was 111 in NanoFMT group, which was remarkably higher than the number of 24 in FMT group and 18 in PBS group. Ternary phase diagram describes the ratio relationship of different attributes in three groups, demonstrating the much higher relative abundance of gut microbiota from NanoFMT group than those of the other two groups (Figure 6B). Shannon index rarefaction curve shows microbial diversity analyzed with different number of sequences. The largest Shannon index indicated the best diverse in terms of species in NanoFMT group (Figure 6C). No significant difference in alpha diversity was found between the PBS and FMT groups, but a larger alpha diversity was obviously present in NanoFMT group (Figures 6D-F). Beta diversity showed that microbiota profiles of NanoFMT group were distinctly separated from that of the other groups (Figures 6G-I). The clustering tree shows the similarity between samples. Samples from FMT group and PBS group presented a certain similarity, while both of them were evidently different from the samples of NanoFMT group (Figure 6J). Significantly, we found that *Salmonella* existed each sample from the FMT and PBS groups, while it was nearly extinct in

NanoFMT group (Figures 6K-L and Figure S19). The result indicated that NanoFMT more thoroughly obliterated infection source *Salmonella*. *Escherichia*, a highly virulent pathogen in *Proteobacteria* [38], could not be found in NanoFMT group, but heavily enriched in the PBS group (Figure 6M). Conversely, some beneficial bacteria enriched in NanoFMT group. *Blautia* can decrease the content of inflammatory cytokines [39]. *Mucispirillum* is responsible for repairing intestinal mucosa by colonization in colon [40]. The relative abundance of these bacteria significantly increased in NanoFMT group, relative to the FMT and PBS groups (Figures 6N-O). Consistent with germ-free mice experiment, the relative abundance of *Lachnospiraceae* in NanoFMT group was 205.0 folds and 118.2 folds higher than that of PBS and FMT groups, respectively (Figure 6P). BugBase phenotype prediction present the relative abundance of aerobic, facultatively anaerobic, anaerobic, forms biofilms and potentially pathogenic bacteria (Figure S20). Biofilms is the important feature of pathogenic bacteria [41]. The highest relative abundance of potentially pathogenic bacteria and biofilms bacteria were both found in PBS group, while NanoFMT group presented the lowest relative abundance (Figure S21). These results demonstrated the excellent regulation on gut microbiota by NanoFMT.

We evaluated the therapeutic effect of NanoFMT on a DSS-induced colitis for verifying the general applicability of NanoFMT against IBD. Mice were fed with 3% DSS for 7 days to develop colitis, and then orally administered with gut microbiota nanocapsules or nude gut microbiota daily for treating 5 days, subsequently sacrificed

to obtain intestinal tissues and serum (Figure 7A). Colon length was significantly prolonged by the treatment of NanoFMT, indicating that NanoFMT alleviated inflammation-induced tissue contraction, in a more pronounced manner than FMT (Figures 7B-C). Furthermore, NanoFMT showed the superior performance on reversing the cytokine levels of IL-1β and interleukin-10 (IL-10) (Figures 7D-E). Intestinal permeability was also ameliorated by NanoFMT (Figure S22), which could be resulted from the combination effects of the modulated gut microbiota and the reversed inflammation. H&E and MPO staining demonstrated that NanoFMT mitigated the inflammatory responses, oedema and reduced MPO positive cells in the intestine, with the best effect among all the treatment groups (Figure 7F). Therefore, NanoFMT could be used as an all-purpose strategy to replace the current FMT for treating IBD.

Finally, the biosafety of NanoFMT was assessed (Figure 7G). Mice was orally administrated daily with or without Nanocapsules protected microbiota for 14 days. Subsequently, blood and organ were respectively harvested for hematological analysis and histopathology analysis (Figures 7H-I and Figure S23). Interestingly, no evident difference was found between NanoFMT group and control group, indicating in vivo toxicity of NanoFMT could be neglected.

Discussion

The reversion of gut microbiota dysbiosis and the remission of intrinsic inflammation are critical for treating IBD [42]. The current therapeutics, including drugs and microbes were unmet need for effective treatment of IBD [43]. Here we

proposed a novel NanoFMT based on microbiota regulation and anti-inflammation. In this system, nanocapsules were firstly constructed by silk fibroin and phosphatidylcholine, and well coated on the surface of single microbes, including gram-negative bacteria, gram-positive bacteria and fungi (Figure 1). Interestingly, gut microbiota nanocapsules were successfully established. Nanocapsules significantly ameliorated gastrointestinal tolerance of gut microbiota and intestinal adhesion, and concurrently rendered extra anti-inflammation effect, but no impacting the growth and proliferation of microbes (Figure 2). Compared with FMT, NanoFMT assisted by nanocapsules greatly improved the diversity and abundance of gut microbiota in germ free mice and perfectly eliminated pathogenic bacteria in mouse model of colitis, which was mainly benefited from the protection of nanocapsules (Figures 3 and 6). Interestingly, typical beneficial bacteria also increased in NanoFMT groups versus FMT group, perhaps contributing to the microbiota balance and inflammation reduction. The excellent efficacy of NanoFMT was demonstrated in different colitis models. Importantly, both silk fibroin and phosphatidylcholine were FDA approved materials. Silk fibroin, a strong antioxidant, could eliminate ROS by own β-sheet structures and corresponding peptides, while phosphatidylcholine could inhibit inflammation by protecting the integrity and function of cell members [44, 45]. Therefore, silk and phosphatidylcholine adjusted the ROS and NO level of macrophage (Figure 3), and mitigated intestinal inflammation level in mice (Figures 5 and 7). In brief, NanoFMT, as an effective and safe therapy, presented well clinical prospect for IBD treatment

assisted from the inherent anti-inflammation of nanocapsules components.

Recent studies indicated that FMT manifested unique advantages in the treatment of refractory disease, recurrent disease and chronic disease, such as *clostridium difficile* infection [46]. In 2021, Science reported that PD-1 therapy responder derived FMT together with anti-PD-1 was used for treating patients with PD-1-refractory melanoma, presenting clinical benefit in 6 of 15 patients [7]. In another clinic trial, FMT was used to decolonize multidrug-resistant organism in renal transplant recipients. FMT-treated participants had longer time to recurrent infection versus controls who were not treated with FMT [47]. These studies confirmed the promising application of FMT for the treatment of various diseases. The gastrointestinal tolerance and intestinal adhesion of NanoFMT was prior to common FMT, perhaps achieving better clinical outcomes. However, many challenges still need to be addressed before clinical application, such as the activity stability of microbiota during long-term storage, the establishment of standardized production process, etc.

Conclusion

In summary, we report a new FMT technology based on nanomaterials, in the form of NanoFMT, to improve the delivery style of current FMT for IBD. Silk fibroin and phosphatidylcholine could rapidly form nanoshell via a layer-by-layer approach on each cell from gut microbiota to fabricate single-cell nanocapsules. The single-cell nanocapsules of microbiota showed protective effects from gastrointestinal environment during oral administration, achieving excellent delivery efficiency into the

intestines without impacting microbiota proliferation. NanoFMT presents better alpha and beta diversity of microbiota structure in germ-free mice and superior anti-inflammation in mouse model of colitis than common FMT. Compared with the invasive administration of microbiota slurries and cumbersome preparation of capsules in current FMT, NanoFMT manifested oral convenience, ease preparation and excellent efficacy. Overall, this study provided a safety and novel strategy for improving current FMT treatment assisted by nanomedicine, portending great clinical application prospect.

Abbreviations

AFM: Atom force microscopy; CA: Cholic acid; CCK8: Cell counting Kit-8; CFU: Colony forming units; CGMCC: China General Microbiological Culture Collection center; DSS: Dextran sulphate sodium; DAPI: 4′,6-diamidino-2-phenylindole dihydrochloride; EcN; *Escherichia coli* Nissle 1917; FDA: Food and Drug Administration; FITC: Fluorescein isothiocyanate; FMT: Fecal microbiota transplantation; GF: Germ-free; H&E: Hematoxylin and eosin; IBD: Inflammatory bowel disease; IVIS: In vivo imaging system; LPS: Lipopolysaccharide; MPO: Myeloperoxidase; MTT: Thiazolyl blue; NanoEcN: Silk fibroin and phosphatidylcholine coated *Escherichia coli* Nissle 1917; NanoFMT: Fecal microbiota transplantation assisted by single-cell nanocapsules; OTUs: Operational taxonomic units; PA: *Pediococcus acidilactici*; SC: *Saccharomyces cerevisiae*; SGF: Simulated gastric fluid; SIF: Simulated intestinal fluid; STm: *Salmonella typhimurium*; TEM: Transmission electron microscopy.

Supporting Information

Supporting Information is available from Online Library or the author.

Acknowledgements

Not application.

Author contributions

WLH, JJL, RBW and HLQ designed the whole project and wrote the manuscript. WLH, YC, JFW and FY performed the most of the experiments. JHW, NG and HW performed the animal experiments. ZYW and RY contributed to the investigation. XQL, CLM and QYC contributed to the methodology. All authors read and approved the final manuscript.

Funding

This work was financially supported by the National Natural Science Foundation of China (32100070; 32260020; 81730102), the Science and Technology Commission of Shanghai Municipality (YDZX20213100003690), the Shanghai Municipal Health Bureau (ZHYY-ZXYJHZX-202105), the Shanghai Hospital Development Center (SHDC2022CRS041), the Supported by the Fundamental Research Funds for the Central Universities (22120220607), the Startup Funding of Hainan University (KYQD(ZR)21200), the Science and Technology Development Fund (FDCT) of Macau SAR (SKL-QRCM(UM)-2023-2025, 005/2023/SKL, 0086/2022/A2 and 0065/2021/A2), and Shenzhen Science and Technology Innovation Commission (EF023/ICMS-WRB/2022/SZSTIC).

Data availability

The data and materials used in the current study are all available from the corresponding author upon reasonable request.

Declarations

Ethics approval and consent to participate

All in vivo animal experiments were conducted with the guidelines of the Shanghai Medical Experimental Animal Care. Animal protocols were approved by the Institutional Animal Care and Use Committee of Shanghai Tenth People Hospital (SHDSYY-2021-6483).

Consent for publication

Not applicable.

Competing interests

The authors declare no competing interests.

References

1. Agirman G, Hsiao EY. Gut microbes shape athletic motivation. Nature. 2022; 612: 633-4.
2. Almeida A, Mitchell AL, Boland M, Forster SC, Gloor GB, Tarkowska A, et al. A new genomic blueprint of the human gut microbiota. Nature. 2019; 568: 499-504.
3. Erdmann J. How gut bacteria could boost cancer treatments. Nature. 2022; 607: 436-9.
4. Hanssen NMJ, de Vos WM, Nieuwdorp M. Fecal microbiota transplantation in human metabolic diseases: From a murky past to a bright future? Cell Metab. 2021; 33: 1098-110.
5. Mocanu V, Zhang Z, Deehan EC, Kao DH, Hotte N, Karmali S, et al. Fecal microbial transplantation and fiber supplementation in patients with severe obesity and metabolic syndrome: a randomized double-blind, placebo-controlled phase 2 trial. Nat Med. 2021; 27: 1272-9.
6. Olesen SW, Leier MM, Alm EJ, Kahn SA. Searching for superstool: maximizing

the therapeutic potential of FMT. Nat Rev Gastroenterol Hepatol. 2018; 15: 387-8.
7. Davar D, Dzutsev AK, McCulloch JA, Rodrigues RR, Chauvin JM, Morrison RM, et al. Fecal microbiota transplant overcomes resistance to anti-PD-1 therapy in melanoma patients. Science. 2021; 371: 595-602.
8. Hamilton MJ, Weingarden AR, Sadowsky MJ, Khoruts A. Standardized frozen preparation for transplantation of fecal microbiota for recurrent Clostridium difficile infection. Am J Gastroenterol. 2012; 107: 761-7.
9. Thaiss CA, Zeevi D, Levy M, Zilberman-Schapira G, Suez J, Tengeler AC, et al. Transkingdom control of microbiota diurnal oscillations promotes metabolic homeostasis. Cell. 2014; 159: 514-29.
10. Schmidt TSB, Li SS, Maistrenko OM, Akanni W, Coelho LP, Dolai S, et al. Drivers and determinants of strain dynamics following fecal microbiota transplantation. Nat Med. 2022; 28: 1902-12.
11. Rinott E, Youngster I, Yaskolka Meir A, Tsaban G, Zelicha H, Kaplan A, et al. Effects of diet-modulated autologous fecal microbiota transplantation on weight regain. Gastroenterology. 2021; 160: 158-73.
12. Haifer C, Paramsothy S, Kaakoush NO, Saikal A, Ghaly S, Yang T, et al. Lyophilised oral faecal microbiota transplantation for ulcerative colitis (LOTUS): a randomised, double-blind, placebo-controlled trial. Lancet Gastroenterol Hepatol. 2022; 7: 141-51.
13. Serrano-Villar S, Talavera-Rodriguez A, Gosalbes MJ, Madrid N, Perez-Molina JA, Elliott RJ, et al. Fecal microbiota transplantation in HIV: A pilot placebo-controlled study. Nat Commun. 2021; 12: 1139.
14. Jiang ZD, Ajami NJ, Petrosino JF, Jun G, Hanis CL, Shah M, et al. Randomised clinical trial: faecal microbiota transplantation for recurrent Clostridum difficile infection - fresh, or frozen, or lyophilised microbiota from a small pool of healthy donors delivered by colonoscopy. Aliment Pharmacol Ther. 2017; 45: 899-908.
15. Xue K, Wang L, Liu J. Surface modification of bacteria to optimize immunomodulation for advanced immunotherapy. ChemMedChem. 2023; 18: e202200574.
16. Wang J, Guo N, Hou W, Qin H. Coating bacteria for anti-tumor therapy. Front Bioeng Biotechnol. 2022; 10: 1020020.
17. Gurbatri CR, Arpaia N, Danino T. Engineering bacteria as interactive cancer therapies. Science. 2022; 378: 858-64.
18. Huang K, Liu W, Wei W, Zhao Y, Zhuang P, Wang X, et al. Photothermal hydrogel encapsulating intelligently bacteria-capturing Bio-MOF for infectious wound healing. ACS Nano. 2022; 16: 19491-508.
19. Qiu M, Tang Y, Chen J, Muriph R, Ye Z, Huang C, et al. Lung-selective mRNA delivery of synthetic lipid nanoparticles for the treatment of pulmonary lymphangioleiomyomatosis. Proc Natl Acad Sci U S A. 2022; 119.
20. Li J, Hou W, Lin S, Wang L, Pan C, Wu F, et al. Polydopamine nanoparticle-mediated dopaminergic immunoregulation in colitis. Adv Sci (Weinh). 2022; 9:

e2104006.
21. Luo H, Chen Y, Kuang X, Wang X, Yang F, Cao Z, et al. Chemical reaction-mediated covalent localization of bacteria. Nat Commun. 2022; 13: 7808.
22. Hou W, Li J, Cao Z, Lin S, Pan C, Pang Y, et al. Decorating bacteria with a therapeutic nanocoating for synergistically enhanced biotherapy. Small. 2021; 17: e2101810.
23. Li J, Xia Q, Guo H, Fu Z, Liu Y, Lin S, et al. Decorating bacteria with triple immune nanoactivators generates tumor-resident living immunotherapeutics. Angew Chem Int Ed Engl. 2022; 61: e202202409.
24. Baek J, Ramasamy M, Cho DG, Soo CCC, Kapar S, Lee JY, et al. A new approach for the encapsulation of using shellac and cellulose nanocrystals. Food Hydrocolloid. 2023; 134: 108079.
25. Zhou J, Li M, Chen Q, Li X, Chen L, Dong Z, et al. Programmable probiotics modulate inflammation and gut microbiota for inflammatory bowel disease treatment after effective oral delivery. Nat Commun. 2022; 13: 3432.
26. Quispe-Tintaya W, Chandra D, Jahangir A, Harris M, Casadevall A, Dadachova E, et al. Nontoxic radioactive Listeria(at) is a highly effective therapy against metastatic pancreatic cancer. Proc Natl Acad Sci U S A. 2013; 110: 8668-73.
27. Wu X, Liu J, Liu Z, Gong G, Zha J. Microbial cell surface engineering for high-level synthesis of bio-products. Biotechnol Adv. 2022; 55: 107912.
28. Phillips DM, Drummy LF, Conrady DG, Fox DM, Naik RR, Stone MO, et al. Dissolution and regeneration of Bombyx mori silk fibroin using ionic liquids. J Am Chem Soc. 2004; 126: 14350-1.
29. Lin S, Mukherjee S, Li J, Hou W, Pan C, Liu J. Mucosal immunity-mediated modulation of the gut microbiome by oral delivery of probiotics into Peyer's patches. Sci Adv. 2021; 7: eabf0677.
30. Sahoo JK, Hasturk O, Falcucci T, Kaplan DL. Silk chemistry and biomedical material designs. Nat Rev Chem. 2023; 7: 302-18.
31. Stremmel W, Merle U, Zahn A, Autschbach F, Hinz U, Ehehalt R. Retarded release phosphatidylcholine benefits patients with chronic active ulcerative colitis. Gut. 2005; 54: 966-71.
32. Fernandes MR, Aggarwal P, Costa RGF, Cole AM, Trinchieri G. Targeting the gut microbiota for cancer therapy. Nat Rev Cancer. 2022; 22: 703-22.
33. Drachuk I, Shchepelina O, Harbaugh S, Kelley-Loughnane N, Stone M, Tsukruk VV. Cell surface engineering with edible protein nanoshells. Small. 2013; 9: 3128-37.
34. Mu H, Bai H, Sun F, Liu Y, Lu C, Qiu Y, et al. Pathogen-targeting glycovesicles as a therapy for salmonellosis. Nat Commun. 2019; 10: 4039.
35. Cui Y, Zhang L, Wang X, Yi Y, Shan Y, Liu B, et al. Roles of intestinal Parabacteroides in human health and diseases. FEMS Microbiol Lett. 2022; 369: fnac072.
36. Tian Y, Xu J, Li Y, Zhao R, Du S, Lv C, et al. MicroRNA-31 reduces inflammatory signaling and promotes regeneration in colon epithelium, and delivery

of mimics in microspheres reduces colitis in mice. Gastroenterology. 2019; 156: 2281-96.
37. Gou S, Huang Y, Wan Y, Ma Y, Zhou X, Tong X, et al. Multi-bioresponsive silk fibroin-based nanoparticles with on-demand cytoplasmic drug release capacity for CD44-targeted alleviation of ulcerative colitis. Biomaterials. 2019; 212: 39-54.
38. Han C, Dai Y, Liu B, Wang L, Wang J, Zhang J. Diversity analysis of intestinal microflora between healthy and diarrheal neonatal piglets from the same litter in different regions. Anaerobe. 2019; 55: 136-41.
39. Ozato N, Saito S, Yamaguchi T, Katashima M, Tokuda I, Sawada K, et al. Blautia genus associated with visceral fat accumulation in adults 20-76 years of age. NPJ Biofilms Microbiomes. 2019; 5: 28.
40. Herp S, Brugiroux S, Garzetti D, Ring D, Jochum LM, Beutler M, et al. Mucispirillum schaedleri antagonizes salmonella virulence to protect mice against colitis. Cell Host Microbe. 2019; 25: 681-94.
41. Songtanin B, Peterson CJ, Molehin AJ, Nugent K. Biofilms and benign colonic diseases. Int J Mol Sci. 2022; 23: 14259.
42. Cai L, Chen G, Wang Y, Zhao C, Shang L, Zhao Y. Boston ivy-inspired disc-like adhesive microparticles for drug delivery. Research (Wash D C). 2021; 2021: 9895674.
43. de Souza HSP, Fiocchi C, Iliopoulos D. The IBD interactome: an integrated view of aetiology, pathogenesis and therapy. Nat Rev Gastroenterol Hepatol. 2017; 14: 739-49.
44. Ai RJ, Xu J, Ji GZ, Cui BT. Exploring the phosphatidylcholine in inflammatory bowel disease: potential mechanisms and therapeutic interventions. Curr Pharm Des. 2022; 28: 3486-91.
45. Qian ZY, Sun C, Li QQ, Xie YF, Zhan LP, Liu XL, et al. Unravelling the antioxidant behaviour of self-assembly β-Sheet in silk fibroin. Redox Biol. 2024; 76: 103307.
46. Habibi S, Rashidi A. Fecal microbiota transplantation in hematopoietic cell transplant and cellular therapy recipients: lessons learned and the path forward. Gut Microbes. 2023; 15: 2229567.
47. Woodworth MH, Conrad RE, Haldopoulos M, Pouch SM, Babiker A, Mehta AK, et al. Fecal microbiota transplantation promotes reduction of antimicrobial resistance by strain replacement. Sci Transl Med. 2023; 15: eabo2750.

Figure Captures

Figure 1 Schematic illustration of single-cell nanocapsules for FMT (NanoFMT).

Figure 2 Preparation of single-cell nanocapsules of gut microbiota. EcN, PA, SC and microbiota were coated by coincubation with 0.1% (w/v) silk fibroin under shaking at 35 rpm for 10 min before being resuspended in 0.1 M K^+ phosphate buffer with vigorously vortexing for 10 min. Silk fibroin coated cells were centrifugated, washed and resuspended in 5 mg/mL phosphatidylcholine and incubated by vigorous shaking for 10 min. The final coated cells were named as NanoEcN, NanoPA, NanoSC and NanoMicrobiota. (A-C) Size distribution of microbes and their nanoderivatives. (D-E) Zeta potentials of microbes and their nanoderivatives. (G) Representative TEM images of microbes and their nanoderivatives. Scale bar: 500 nm (EcN, NanoEcN, PA and NanoPA) or 2 μm (SC and NanoSC). (H) Typical confocal images of microbes and their nanoderivatives. Green and red channels indicate silk fibroin labeled by FITC and phosphatidylcholine labeled by rhodamine B, respectively. Scale bar: 10 μm or 25 μm (NanoSC). (I) Flow cytometric analysis of microbes and their nanoderivatives.

Figure 3 The impact of Nanocapsules on the resistance of environmental assaults, intestinal adhesion and anti-inflammation. (A-D) Growth curves of nanocapsules coated EcN, PA, SC and microbiota respectively at 37 ℃ and 200 rpm. (E-H) The survived numbers of nanocapsules coated EcN, PA, SC and microbiota respectively after exposure to SGF (pH 2.5) supplemented with pepsin for two hours at 37 ℃ and 200 rpm. (I) TEM images of nanocapsules coated EcN, PA, SC and microbiota after exposure to SGF for two hours. (J, K) Typical confocal images (J) and bacterial count (K) of nanocapsules coated EcN after adhesion with the DSS-damaged intestines for 30 min. Blue and red channels indicate intestinal epithelial cells labeled by DAPI and EcN with mCherry fluoreschence, respectively. Scale bar: 10 μm. (L-O) Anti-inflammatory properties of the nanocapsules constituents (silk fibroin and phosphatidylcholine) by analyzing the ROS level (L, M), NO content (N) and percentages of CD86+ macrophages (O) in RAW 264.7 cells. Blue and green channels indicate RAW 264.7 cells labeled by DAPI and ROS labeled by DCFH-DA probe, respectively. Scale bar:

10 μm. Error bars represent standard error of mean (n = 3). $p< 0.05$, *, $p < 0.01$, **, $p < 0.001$, ***.

Figure 4 Nanocapsules mediated intestinal colonization in SPF mice and gut microbiota distribution in germ-free mice. (A) The experimental design for evaluating in vivo resistance of NanoEcN against insults within the GI tract in SPF Balb/c mice. Mice were randomly divided into 2 groups (n = 6) and fed with 2×10^7 CFU/mouse EcN or NanoEcN by oral gavage. (B) Typical images captured by IVIS after 4 h post-administration. (C) Quantification of fluorescence intensities in mice. Error bars represent standard error of mean. (D) Representative fluorescent images of the GI tract. (E) Quantification of fluorescence intensities of the GI tract. (F-H) Bacterial count of EcN in small intestine (F), cecum (G) and colon (H). (I) Type images of EcN colony in small intestine, cecum and colon. (J) The experimental design of FMT to evaluate gut microbiota distribution in germ-free mice. Mice were randomly divided into 2 groups (n = 4) and treated with FMT (2×10^6 CFU/mouse) or NanoFMT (2×10^6 CFU/mouse). (K) Venn diagram of gut microbiota after 24 h NanoFMT. (L) ACE index represent alpha diversity analysis of gut microbiota. Error bars represent standard error of mean. (M) PCA index represent beta diversity analysis of gut microbiota. (N, O) Abundances of phylum (N) and genus (O) in gut microbiota. (P-R) Abundances of Bacteroides (P), Lachnospiraceae (Q) and Parabacteroides (R) in gut microbiota. $p< 0.05$, *, $p < 0.01$, **, $p < 0.001$, ***.

Figure 5 Therapeutic effect of NanoFMT in STm-induced mouse model of colitis. (A) The experimental design for the treatment of STm-induced colitis in mice. Mice were treated with 100 μl of streptomycin solution (200 mg/mL) prior to infection by orally inoculating with 1×10^9 CFU of Salmonella. Mice were randomly divided into 3 groups (n = 5) and treated with PBS, FMT (2×10^7 CFU/mouse/day) and NanoFMT (2×10^7 CFU/mouse/day) at day 2 and 4 post-infection, respectively. All mice were sacrificed for sampling on day 6 post- infection. (B) The survival rate of mice during the treatment. (C) The colon length after treatment. (D, E) The levels of cytokines in

serum measured by commercially available ELISA kits including IL-1β (D) and IL-6 (E). (F) Histopathological images of H&E and MPO stained colon sections. Error bars represent standard error of mean (n = 5). $p< 0.05$, *, $p < 0.01$, **, $p < 0.001$, ***.

Figure 6 Gut microbiota analysis after the treatment of STm-induced mouse model of colitis by NanoFMT. (A) Venn diagram in the OTUs level. (B) Ternary phase diagram in the genus level. (C) Shannon index curve. (D-F) Alpha diversity analysis of gut microbiota presented by ACE index (D), Shannon index (E) and Simpson index (F). (G-I) Beta diversity analysis of gut microbiota presented by PCA analysis (G), PCoA analysis (H) and NMDS analysis (I). (J) UPGMA clustering tree with taxonomic composition. (K) Circos diagram of microbial composition at the genus. (L-P) Abundance of Salmonella (L), Escherichia (M), Blautia (N), Muribaculum (O) and Ruminococcus (P). Error bars represent standard error of mean (n = 5). $p< 0.05$, *, $p < 0.01$, **, $p < 0.001$, ***.

Figure 7 Therapeutic effect of NanoFMT in DSS-induced mouse model of colitis and safety evaluation. (A) The experimental design for the treatment of DSS-induced colitis. Mice were fed with 3% DSS salt in sterile drinking water for 7 days. Mice were randomly divided into 3 groups (n = 5) and then administered with PBS, FMT (2×10^7 CFU/mouse/day) or NanoFMT (2×10^7 CFU/mouse/day) by gavage for 5 days. All mice were sacrificed for sampling on day 6 post-infection. (B) Photographs of colons sectioned from the treated mice. (C) Colon length after treatment. (D, E) Levels of cytokines in serum measured by commercially available ELISA kits including IL-1β (D) and IL-10 (E). (F) Histopathology images of H&E and MPO staining in colon. Error bars represent standard error of mean (n = 5). (G) The experimental design for biosafety evaluation. Mice were randomly divided into 2 groups (n = 6), and orally administrated with PBS or NanoFMT (2×10^7 CFU/mouse/day) daily for 14 days, then sacrificed for pathological analysis. (H) Hematological analysis of mice after biosafety evaluation. (I) Represented H&E

images of heart, liver, spleen, lung and kidney after biosafety evaluation. Error bars represent standard error of mean. $p< 0.05$, *, $p < 0.01$, **, $p < 0.001$, ***.

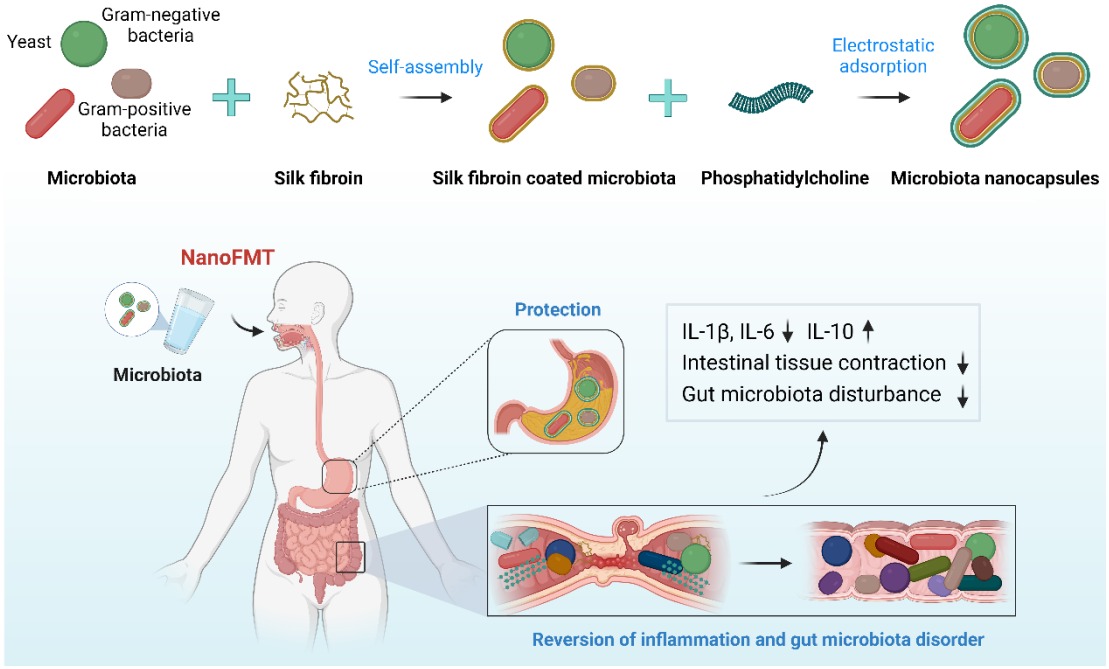

Figure 1 Schematic illustration of single-cell nanocapsules for FMT (NanoFMT).

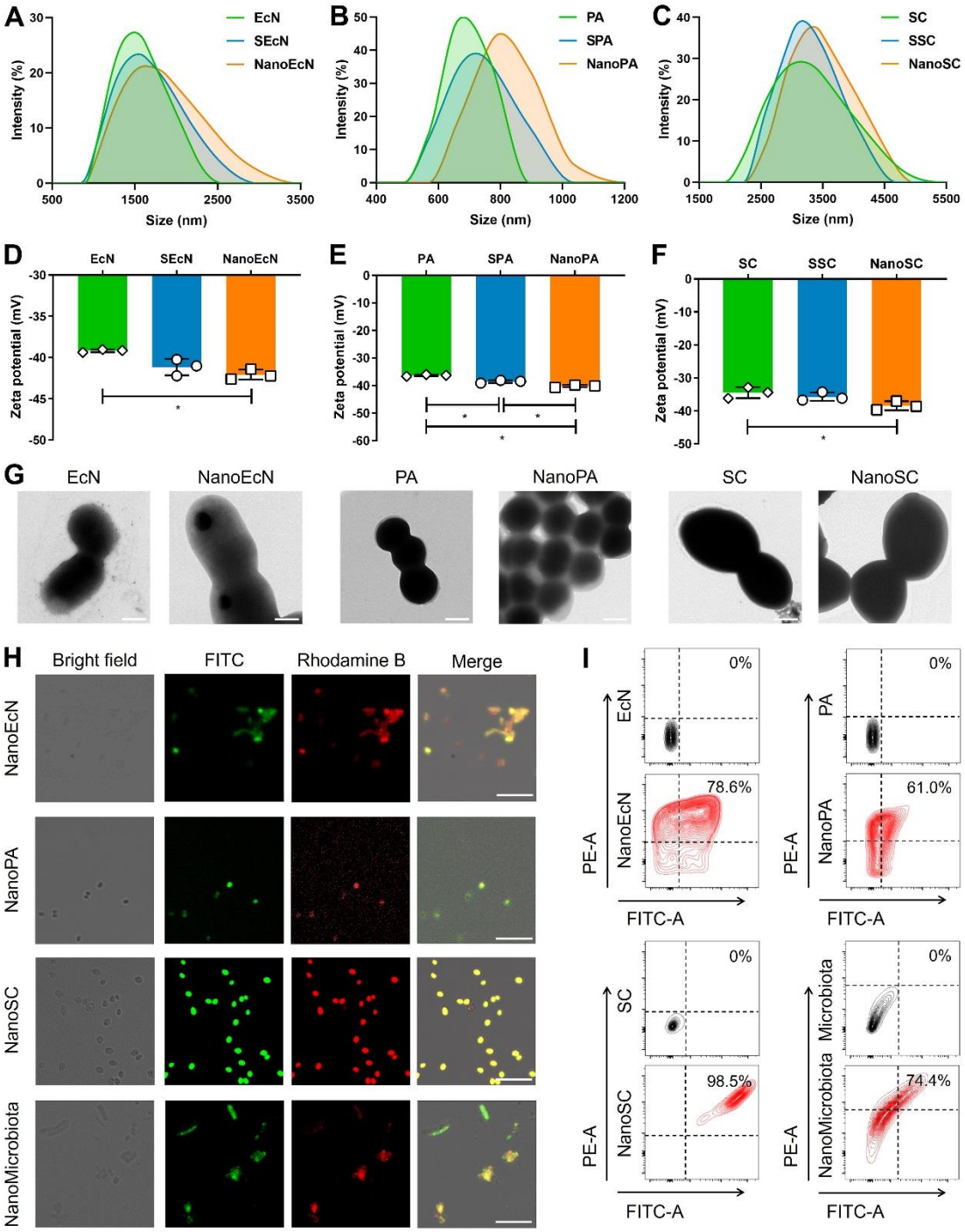

Figure 2 Preparation of single-cell nanocapsules of gut microbiota.

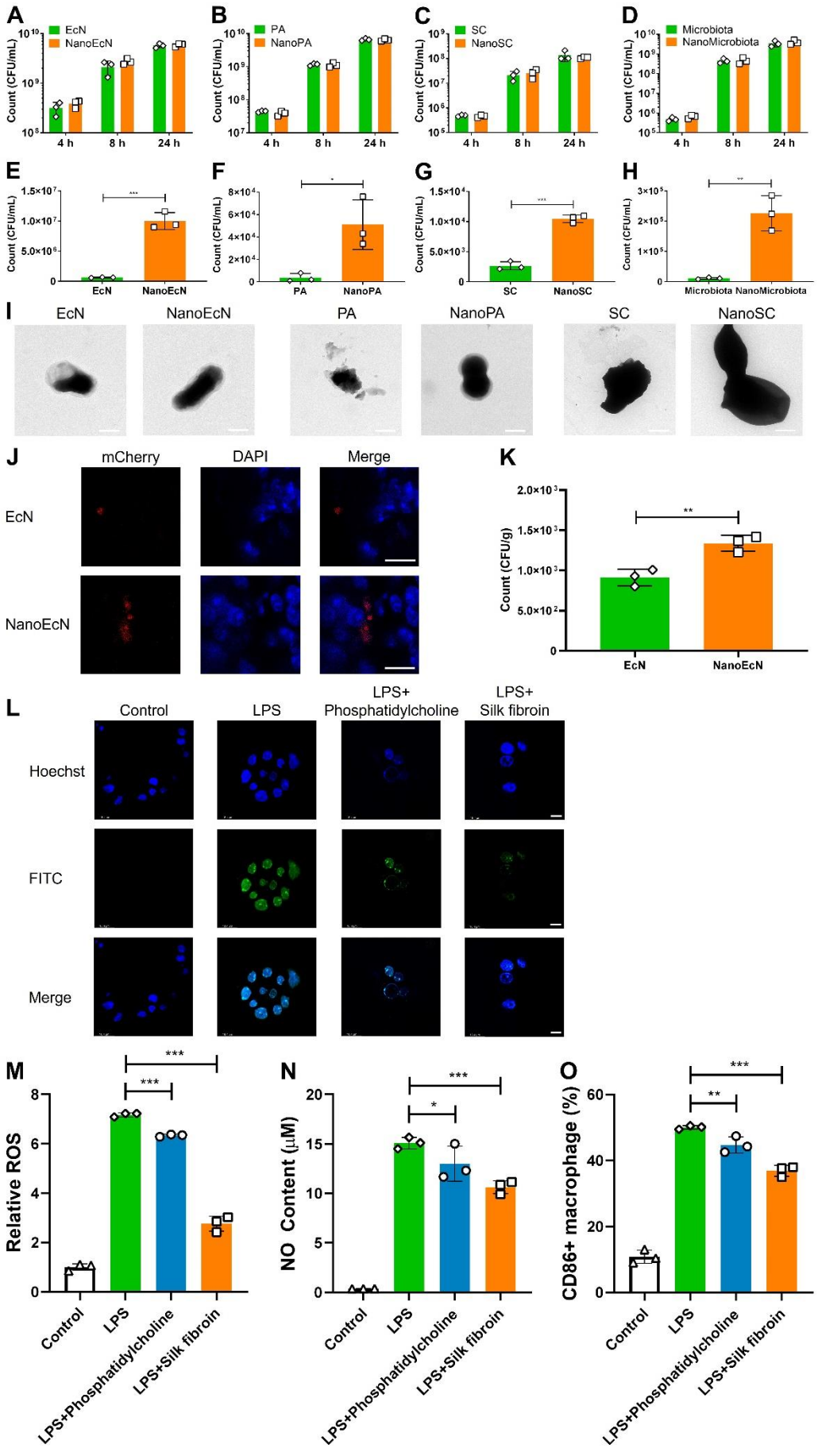
A
EcN
NanoEcN
Count (CFU/mL)
4 h
8 h
24 h
B
PA
NanoPA
C
SC
NanoSC
D
Microbiota
NanoMicrobiota
E
F
G
H
EcN
NanoEcN
PA
NanoPA
SC
NanoSC
Microbiota
NanoMicrobiota
I
J
mCherry
DAPI
Merge
K
Count (CFU/g)
L
Control
LPS
LPS+ Phosphatidylcholine
LPS+ Silk fibroin
Hoechst
FITC
Merge
M
Relative ROS
N
NO Content (μM)
O
CD86+ macrophage (%)

Figure 3 The impact of Nanocapsules on the resistance of environmental assaults, intestinal adhesion and anti-inflammation.

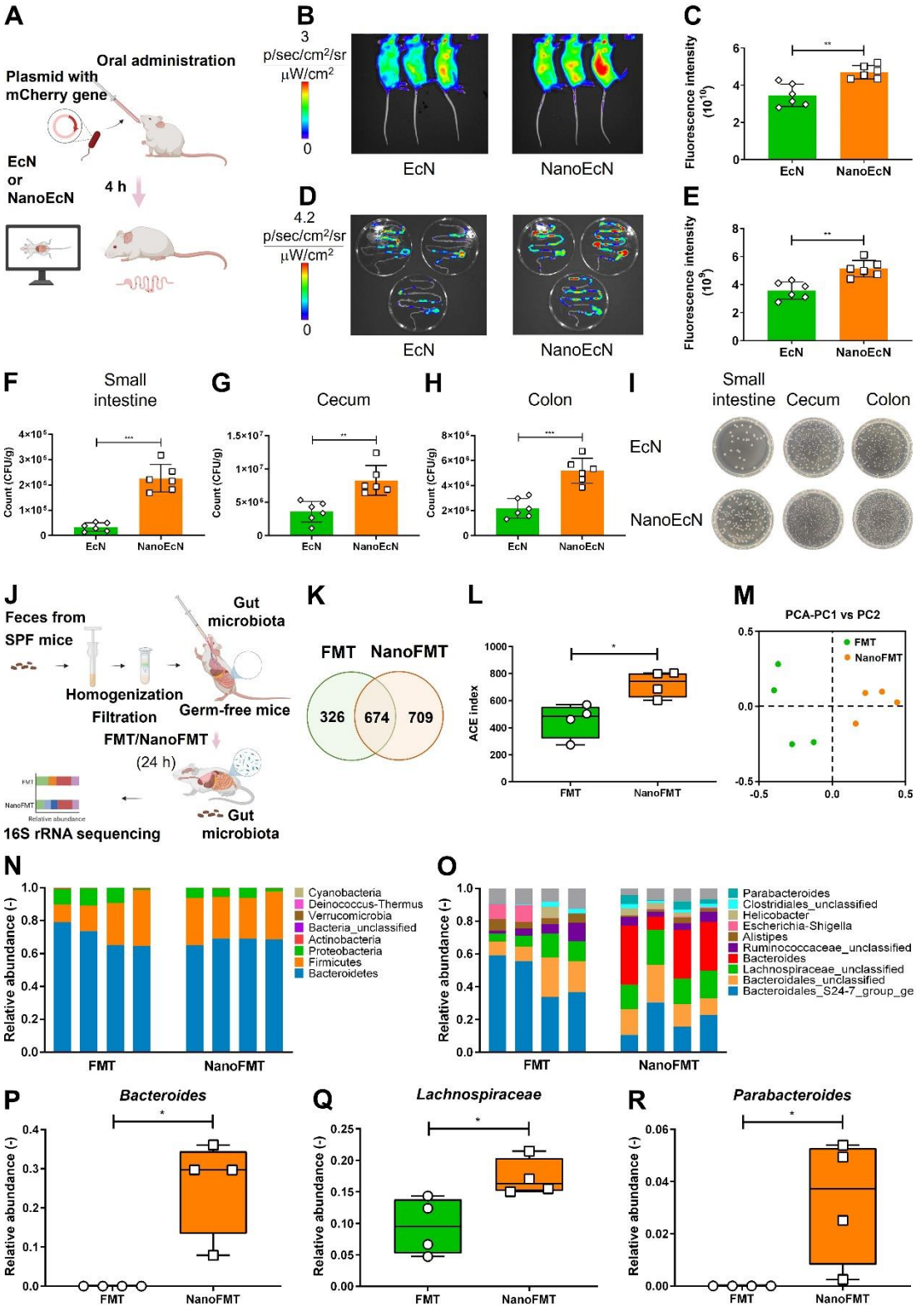

Figure 4 Nanocapsules mediated intestinal colonization in SPF mice and gut microbiota distribution in germ-free mice.

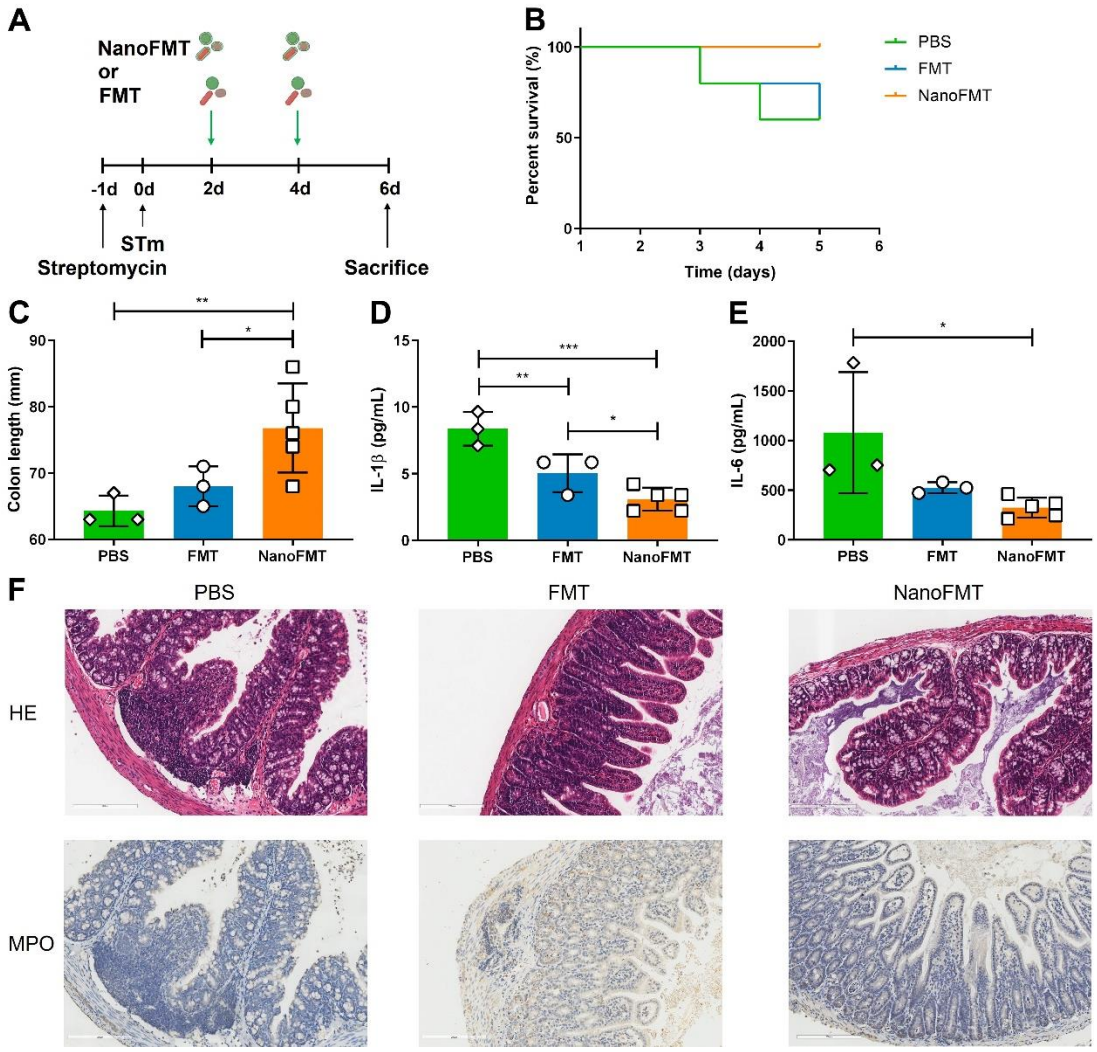

Figure 5 Therapeutic effect of NanoFMT in STm-induced mouse model of colitis.

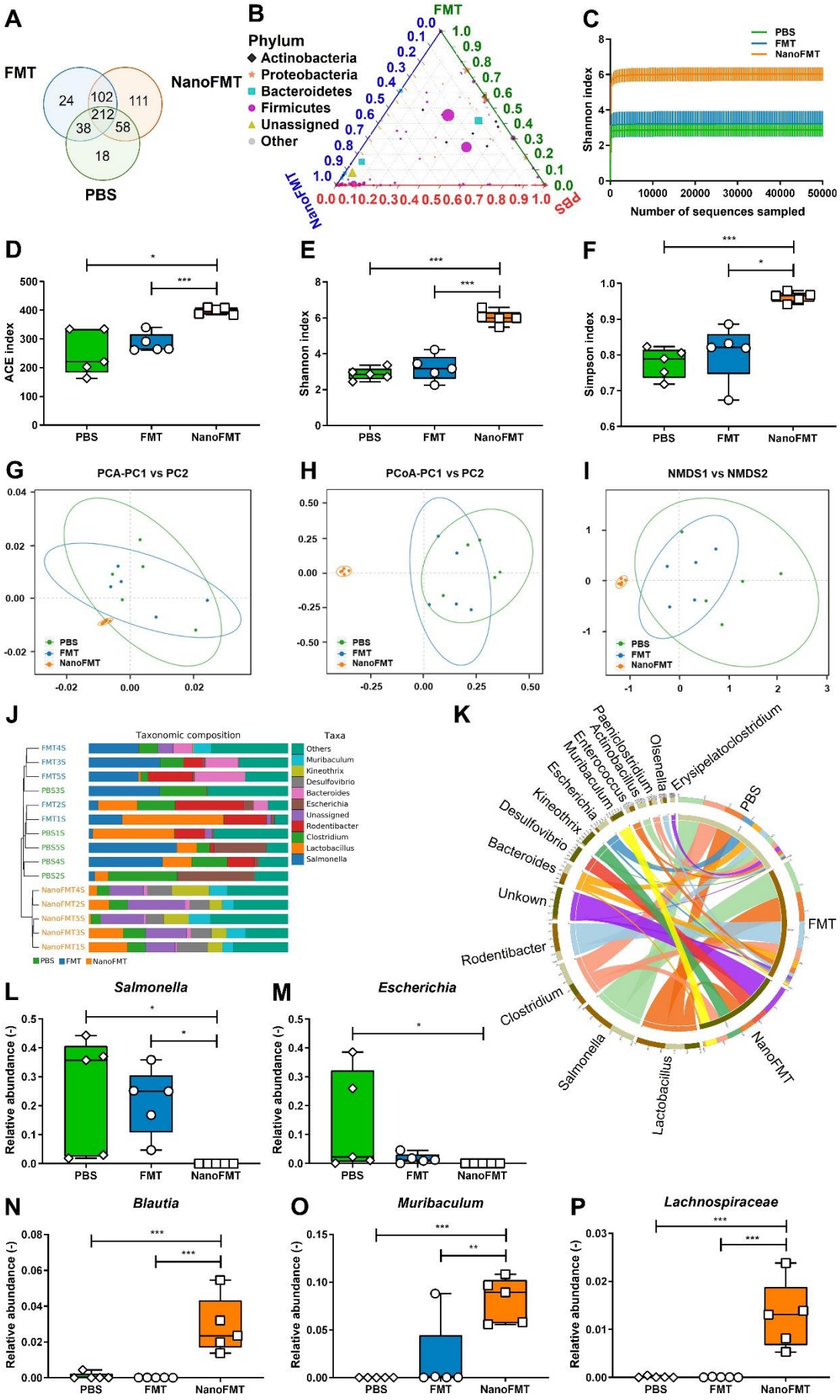
A
FMT
NanoFMT
PBS
24
102
111
212
38
58
18
B
Phylum
Actinobacteria
Proteobacteria
Bacteroidetes
Firmicutes
Unassigned
Other
FMT
NanoFMT
PBS
C
PBS
FMT
NanoFMT
Shannon index
Number of sequences sampled
D
ACE index
E
Shannon index
F
Simpson index
G
PCA-PC1 vs PC2
H
PCoA-PC1 vs PC2
I
NMDS1 vs NMDS2
J
Taxonomic composition
Taxa
Others
Muribaculum
Kineothrix
Desulfovibrio
Bacteroides
Escherichia
Unassigned
Rodentibacter
Clostridium
Lactobacillus
Salmonella
K
Paeniclostridium
Actinobacillus
Enterococcus
Muribaculum
Escherichia
Kineothrix
Desulfovibrio
Bacteroides
Unkown
Rodentibacter
Clostridium
Salmonella
Lactobacillus
Olsenella
Erysipelatoclostridium
PBS
FMT
NanoFMT
L
Salmonella
Relative abundance (-)
M
Escherichia
N
Blautia
O
Muribaculum
P
Lachnospiraceae

Figure 6 Gut microbiota analysis after the treatment of STm-induced mouse model of colitis by NanoFMT.

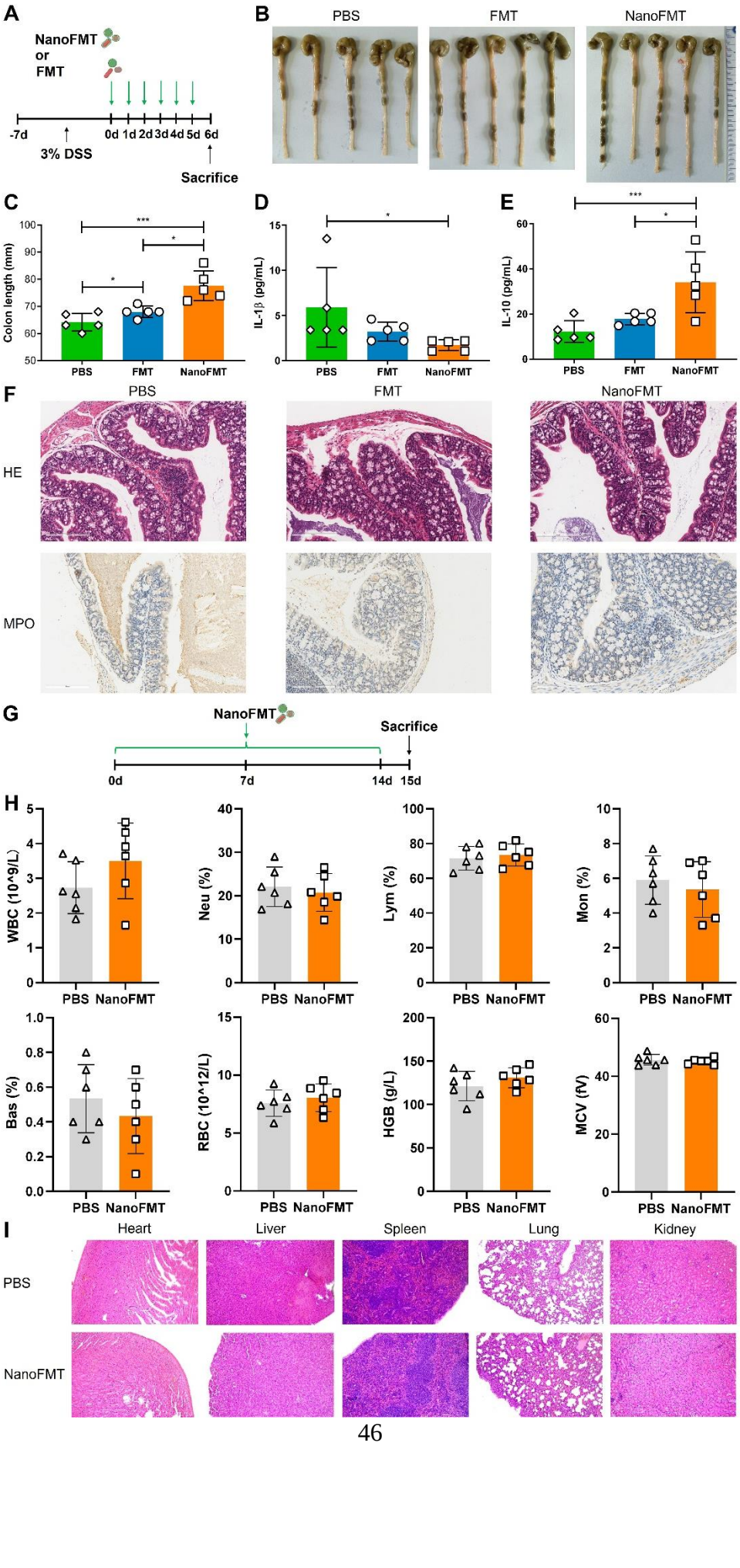
A
NanoFMT
or
FMT
-7d
3% DSS
0d 1d 2d 3d 4d 5d 6d
Sacrifice
B
PBS
FMT
NanoFMT
C
Colon length (mm)
PBS
FMT
NanoFMT
D
IL-1β (pg/mL)
E
IL-10 (pg/mL)
F
HE
MPO
G
NanoFMT
Sacrifice
0d
7d
14d 15d
H
WBC (10^9/L)
Neu (%)
Lym (%)
Mon (%)
Bas (%)
RBC (10^12/L)
HGB (g/L)
MCV (fV)
I
Heart
Liver
Spleen
Lung
Kidney
PBS
NanoFMT

Figure 7 Therapeutic effect of NanoFMT in DSS-induced mouse model of colitis and safety evaluation.